Proceedings of ASME Turbo Expo 2011
GT2011
June 6-10, 2011, Vancouver, British Columbia, Canada

GT2011-45035

AEROELASTICITY AT REVERSED FLOW CONDITIONS - PART 2: APPLICATION TO COMPRESSOR SURGE

Harald Schoenenborn
MTU Aero Engines GmbH
D-80995 Munich, Germany
e-mail: Harald.Schoenenborn@mtu.de

Thomas Breuer
MTU Aero Engines GmbH
D-80995 Munich, Germany
e-mail: Thomas.Breuer@mtu.de

ABSTRACT

The prediction of blade loads during surge is still a challenging task. In literature the blade loading during surge is often referred to as "surge load", which suggests that there is a single source of blade loading. In the second part of the paper it is shown that the "surge load" in reality may consist of two physically different mechanisms: the pressure shock when the pressure breaks down and aeroelastic excitation (flutter) during the blow-down phase in certain cases. This leads to a new understanding of blade loading during surge.

The front block of a multistage compressor is investigated. For some points of the backflow characteristic the quasi steady-state flow conditions are calculated using a RANS-solver. The flow enters at the last blade row, goes backwards through the compressor and leaves the compressor in front of the inlet guide vane. The results show a very complex flow field characterized by large recirculation regions on the suction sides of the airfoils and stagnation regions close to the trailing edges of the airfoils.

Based on these steady solutions unsteady calculations are performed with a linearized aeroelasticity code. It can be shown that some of the rotor stages are aerodynamically unstable in the first torsional mode. Thus, in addition to the pressure shock the blades may be excited by flutter during the surge blow-down phase. In spite of the short blow-down phase typical for aero-engine high pressure compressors, this may lead to very high blade stresses due to high aeroelastic excitation at these special flow conditions.

The analytical results compare very well with the observations during rig testing. The correct nodal diameter of the blade vibration is reproduced and the growth rate of the blade vibration is predicted quite well, as a comparison with tip-timing measurements shows. A new flutter region in the compressor map was detected experimentally and analytically.

NOMENCLATURE

A	Amplitude
f	Blade eigenfrequency
IBPA	Inter-blade phase angle
LE	Leading edge
ND	Nodal diameter
p	Pressure
Ref	Reference
S/G	Strain gauge
stat	Static
T	Vibration period
TE	Trailing edge
t	Time
tot	total
δ	Aerodynamic damping (log. decrement)
1F	First bending vibration mode
1T	First torsional vibration mode

1 INTRODUCTION

In literature the blade loading during surge is often referred to as "surge load", which suggests that there is a single source of blade loading. Figure 1 shows pressure and stress traces recorded during a typical surge event for one rotor blade of a multi-stage compressor. In the upper picture a) the unsteady pressure of a Kulite pressure transducer above the rotor blade is plotted. The red line represents an averaged value derived from low-pass filtering of the original signal.

In the lower picture b) a strain-gauge signal of the same blade is presented. The S/G-signal is filtered so that the single vibration modes can be distinguished. The red line represents the vibration of the first bending mode and the green line that of the first torsional mode.

At time t_1 the pressure spike indicates the occurrence of surge. The pressure spike represents a pressure shock wave which reaches the rotor (sometimes called surge hammershock) leading to a small excitation of the first bending mode. A short time later (in the order of several milliseconds), the blow-down phase starts at t_2 and the pressure of the compressor is falling until at time t_3 the compressor recovers. During this period a sharp increase in the S/G-signal of the first torsional mode can be discerned, which can reach levels above the yield strength of the blade material, leading to a blade failure. The length of the blow-down phase depends on the volume downstream of the compressor and may last between tens of milliseconds up to seconds. Figure 2 shows a picture of a typical blade damage after high power surges. A crack at the airfoil trailing edge indicates a failure due to high vibrations in the first torsional mode.

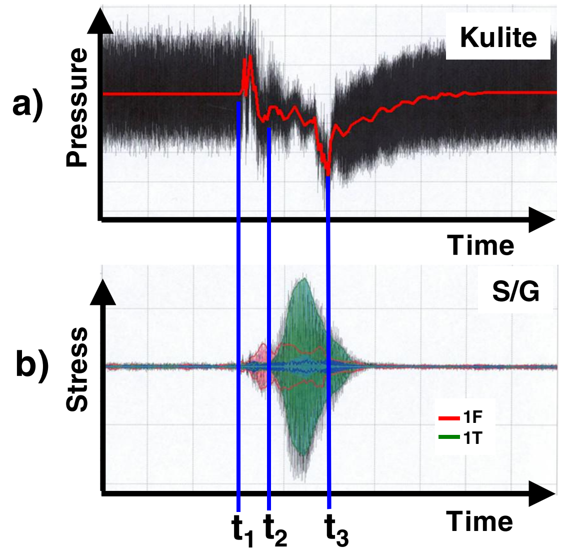

Figure 1: Pressure and stress over a surge cycle

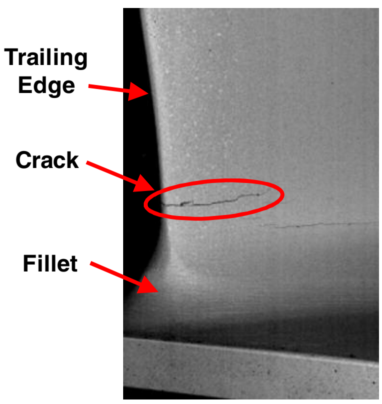

Figure 2: Crack at airfoil trailing edge after surge

Figure 1 clearly shows that there are two physically different mechanisms acting on the blade during the surge. In Figure 3 a sketch of a surge cycle is plotted. When the pressure is increased and the surge line is reached, the pressure wave (hammershock) leads to a first loading of the blade. This is described in some papers, the most important one from Mazzawy [1]. After this, the flow is reversed until the volumes associated with the compressor are empty. This period is much longer and it is during this period when the blades experience another type of loading which is not yet described in literature in detail. When the compressor volumes are empty, the compressor recovers quite fast and returns to the pre-surge operating point. The present paper focuses on this second type of surge blade loading during the phase of reversed flow.

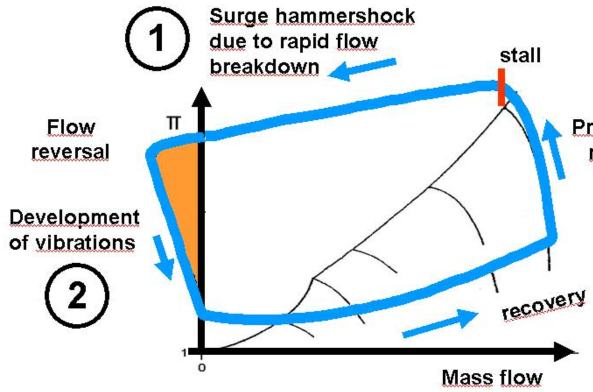

Figure 3: Compressor map and surge cycle

First, a literature survey is given on surge loads. A test is described which has been conceived to investigate the flow conditions during surge and to gather experimental data which helps to understand the physical mechanism stimulating the observed structural vibrations. Then the numerical procedures for the steady flow investigations and the aeroelastic calculations are presented. In the fourth section, the investigation setup is described and the results of the steady calculations are presented. The fifth section presents the unsteady analytical investigations and its comparison to measurements during rig testing can be found in section six. Finally, the paper is summarized. The aim of the paper is to show experimentally and analytically that the second type of surge loading is a flutter behavior which leads to a new understanding of blade loading during surge.

It should be noted that for proprietary reasons only dimensionless figures and numbers can be presented.

Literature surge loads

In Schoenenborn and Breuer [2] an overview of the combined aerodynamic and mechanical effects of surge and its related literature is given. Since then, only few additional publications can be found on this topic. Simmons et al. [3] showed some investigations on blade failures caused by aerodynamic instabilities, including rotating stall and flutter. They reported that a most likely failure of one vane was caused by a combination of excessive wakes from the downstream rotor blades and flutter associated with mild intermittent surge. They assumed that the self-excitation was due to vortex shedding.

Vahdati et al. [4] performed an advanced 3D viscous time-accurate flow analysis of a surge event of a complete core compressor with application to aeroelasticity. They came to the conclusion that the highest forcing corresponds to the surge frequency.

Mailach and Vogeler [5] determined experimentally the blade pressure forces during stall, but not at surge. Longley [6] developed a blockage-mixing method in order to calculate the complex reverse flow behavior during a complete surge cycle. Applying this method for estimating the surge loads he came to the conclusion that the load is correlated to the surge pressure pulse.

Gamache and Greitzer [7] presented detailed measurements of a 3-stage-compressor during surge. The principal flow features during the surge blow-down phase were shown. They found a spinning acoustic disturbance mode over a narrow range of reversed flow conditions, but they did not report anything about blade loading during these complex flow conditions.

In [8] Frodl developed a procedure for the estimation of blade surge loads based on pressure shocks. He determined the distribution of the unsteady forces and momentum and calculated the response of the blade.

Recently, di Mare et al. [9] performed a numerical study of a complete surge cycle of a 6-stage high-pressure compressor, using a 3D time accurate CFD code. For various conditions (steady reversed flow, normal flow, max reversed flow, beginning of surge cycle and zero flow) they performed flutter stability computations of a rotor for some mode shapes. They found that the damping curve (aerodynamic damping vs. IBPA) has still the shape of a sine curve, but that the level of damping is largely reduced compared to normal flow conditions. Only for some points close to an inter-blade phase angle of 0° they found negative damping.

In summary, the majority of publications relate blade loads during surge to the initial hammershock pulse, rather than to flow conditions prevailing during reverse flow. However, as the data presented in Figure 1 suggests, largest vibratory response occurs not as a result of the surge pressure loads, but rather due to a different mechanism. To the author's knowledge, this second mechanism is described for the first time.

2 RIG INVESTIGATIONS

In order to investigate the interaction between flow and structure during surge which leads to the sudden increase of blade vibration, a series of tests has been performed with a multistage compressor. The compressor used for the investigation featured eight stages and is representative of state-of-the-art compressors for either civil or military applications in terms of Mach number and blade loading. All rotors are built as integrally bladed disks (blisks), providing only very little structural damping. The inlet guide vane as well as the first three stator rows are variable to adapt flow conditions and stage matching to optimize performance throughout the speed range.

Apart from the standard steady-state instrumentation used to map overall and stage performance, unsteady pressure transducers in front of the rotors (flush mounted) have been installed to measure transient pressures during surge. Tip timing probes have been incorporated to detect blade vibrations of rotor blades.

Surge has been induced at various speeds up to design speed by closure of the exit throttle. In order to achieve realistic flow conditions during a surge cycle (among others duration of surge), the downstream volume between compressor exit guide vane and throttle has been defined to mimic conditions which the compressor would encounter in an engine.

Surge-induced blade vibrations of the type described in the introductory section have been encountered in the upper speed regime of the compressor. Data collected during these events formed the basis for subsequent investigations to uncover the mechanism driving blade vibrations.

3 NUMERICAL PROCEDURE

The numerical investigations which have been performed used the MTU standard procedure for flutter calculations. This procedure consists of a steady flow solution in combination with a linearized Euler method, which is used subsequently to calculate the unsteady behavior of the airfoil.

Steady Flow Solver

For the steady aerodynamic flow solution the turbo machinery numerical simulation system TRACE [10][11][12], jointly developed by MTU and DLR, is used. It is applied by a growing user community both in research and industry.

In this solver, within the relative frame of reference, the 3-D Reynolds averaged Navier-Stokes equations are integrated in time by a fully implicit formulation of the second-order scheme for the compressible ideal or real gas in conjunction with the two equation k-ω turbulence model, which is enhanced by DLR´s own extensions for rotation, compression and stagnation point anomaly.

The convective fluxes are discretized using the Roe's TVD upwind scheme which is combined with the van Leer's MUSCL extrapolation to obtain second- or third-order accuracy in space depending on the limiter used. The derivatives of the viscous fluxes are approximated by central differences.

For a steady multistage calculation, the nonreflecting formulation according to Giles is applied at inlet and outlet boundaries, whereas the coupling of different blade rows is realized by the so called mixing-plane approach. For more details the reader is referred to the above mentioned references.

Unsteady Flow Solver

The unsteady flow is computed with a time-linearized Euler method. The flow is split into a mean, steady flow and a small, harmonic perturbation. Thus, the steady flow problem is decoupled from the unsteady problem. The steady flow, which is computed with the code described above, is interpolated on a single H-grid for each passage. The time-linear unsteady flow equations are solved on a moving grid, which conforms to the motion of the airfoils. The solution algorithm uses a cell-vertex formulation. Nonreflecting boundary conditions are employed to accurately model isolated cascades.

More details of the linearized method and its extensive validation can be found in Kahl [13] and Kahl and Klose [14].

In the first part of the paper [15], this procedure is applied to the calculation of a compressor cascade under controlled vibration with a constant inter-blade phase angle and amplitude at steady reversed flow conditions. The comparison with steady-state measurements showed excellent agreements. For the unsteady pressure amplitudes and phases, the experimental results compare quite well with the calculations for an IBPA of -180°, which is special interest here, as shown later. The global stability of the configuration was compared by the overall aerodynamic damping coefficient based on the unsteady pressure distribution and phases on the blade. The agreement was found to be quite good, taking into account the relatively large measurement uncertainties on the experimental side and the difficult flow conditions and the linearized solver on the numerical side.

4 INVESTIGATION SETUP AND STEADY FLOW FIELD

The numerical investigation was performed on the front block of the multistage test compressor comprising the Inlet Guide Vane and the rotor and stator blades of the first four stages, as shown in the sketch in Figure 4. The computational grid for this setup consists of 7.364.509 grid points, with the same grid parameters and discretisation as for normal CFD calculations in the design phase.

For the reversed flow analysis, the inlet of the computational domain was set at the exit of the forth stator vane, with a flow angle in negative axial direction. In addition, total pressure and temperature were described. The outlet static pressure was set at the inlet of the Inlet Guide Vane (IGV). The complete front block was simulated as the flow is highly 3-dimensional and it would be very difficult to determine appropriate boundary conditions for a single-passage calculation.

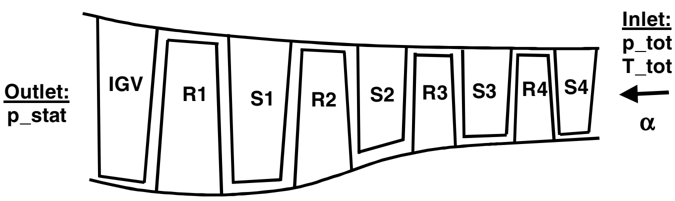

Figure 4: Investigation setup compressor front block

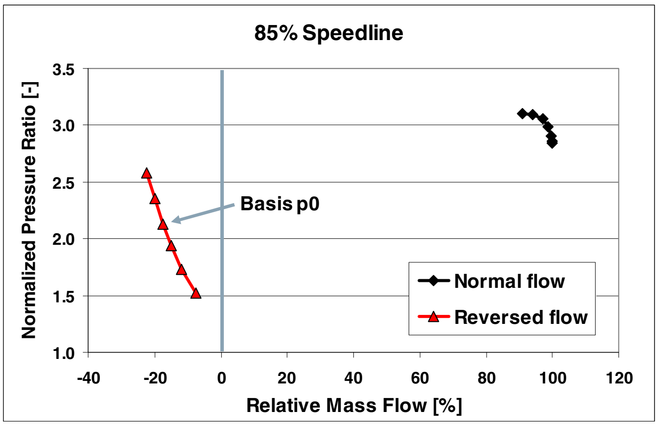

Figure 5: Part compressor map stage 1-4

For 85% speed a speed line on the tertiary characteristic was calculated with the reversed flow analysis. In Figure 5 the normalized pressure ratio over the mass flow rate is plotted. The black line shows the speed line of the front block during normal compressor operation. The red line corresponds to the speed line during reversed flow at this rotor speed. The point “Basis p0” is a reference point which is examined in more detail further below.

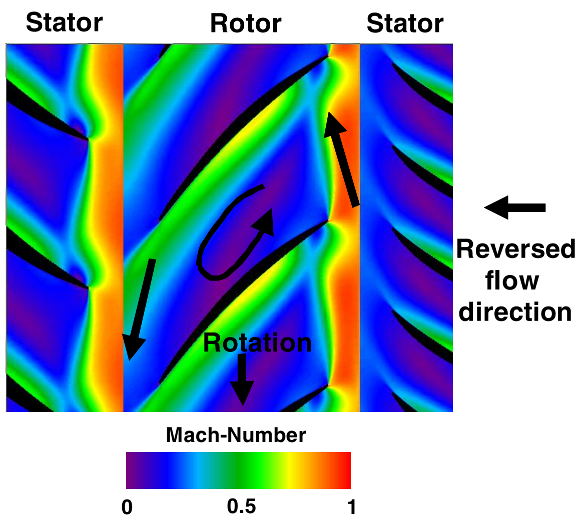

Figure 6: Flow field at backflow conditions of the rotor

In Figure 6 the resulting flow field for one of the rotor blades with the two adjacent stator vanes is presented with contour plots of the relative Mach number at midspan for the basis operating point p0. In the following sections, results for the same rotor stage are always presented. Due to proprietary reasons, only results for one rotor stage can be shown. In the rotor frame, the flow comes straight onto the trailing edge region of the blade with high a Mach number, leading to a huge recirculation region on the suction side of the blade with a low Mach number. Along the pressure side of the rotor, a small region with a higher Mach number can be seen.

It should be kept in mind that during the complete surge cycle the rotor-speed is nearly constant due to the high inertia of the rotor and the short surge period. Thus, the rotor blades are adding energy to the fluid all the time.

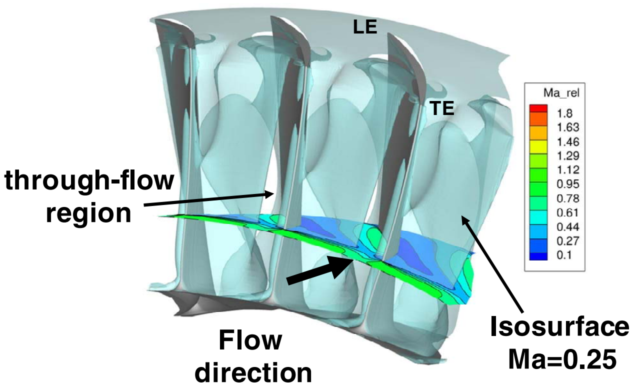

Figure 7: Mach-isosurface at backflow conditions of the rotor

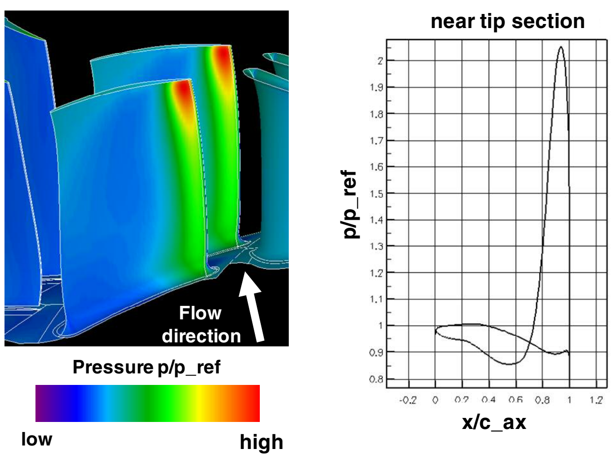

Figure 8: Static pressure distribution at backflow conditions of the rotor

Figure 7 gives a further impression of the complex three-dimensional flow field. Here an isosurface of the relative Mach number (Ma=0.25), which starts close to the trailing edge of the blade, indicates the sizes of the recirculation region. All the flow during the surge blow-down phase goes through the small area close to the pressure side of the airfoil. This flow condition works as a throttle to the complete compressor and explains that the mass flow during the blow-down phase is much smaller than during normal operation. The flow fields of the other stages look quite similar. Overall, there is a quite good agreement with the sketches of the reversed flow conditions in the paper from Gamache and Greitzer [7].

In Figure 8 finally the static pressure distribution on the blade surface of the third rotor is shown. On the left hand side, the contour plot of the dimensionless pressure on the blade surface is presented. On the right hand side the profile pressure at a near tip section is plotted. There is a large stagnation region close to the trailing edge, which becomes higher closer to the tip due to the higher circumferential velocity of the blade, whereas the front part of the blade shows a uniform pressure distribution.

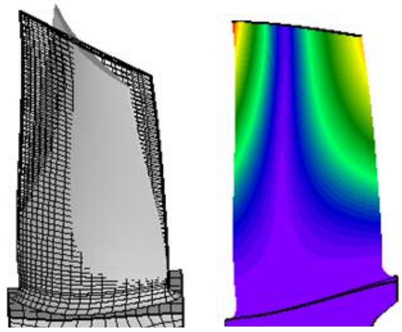

Figure 9: First torsional vibration mode shape of the rotor

5 UNSTEADY FLOW INVESTIGATIONS

Based on the above described complex flow field, unsteady aeroelastic calculations were performed with the linearized Euler code. This is a very common approach for aeroelastic investigations of flutter and forced response. The second eigenmode, which corresponds to the first torsion mode, was investigated for all four rotor blades. As an example, the mode shape of the third rotor is presented in Figure 9.

The rotationary motion of two adjacent airfoils of the rotor blade and the resulting unsteady pressure distribution, in combination with the disturbance flow vectors, is shown in Figure 10 for a complete vibration period at a near tip section for an inter-blade phase angle of 180°, at reversed flow conditions for performance point p0. The movement is enlarged in order to show the effects. The left picture shows the steady pressure and the next eight pictures the unsteady pressure at time steps of 1/8T. The underlying steady flow direction is from right to left.

The arrows indicate the momentary direction of rotation of the blades with positive or negative direction according to the right hand rule and indicated in the right lower corner of the Figure. The red arrow indicates the direction of the movement of blade 1 (upper blade) and the blue arrow that of blade 2 (lower blade).

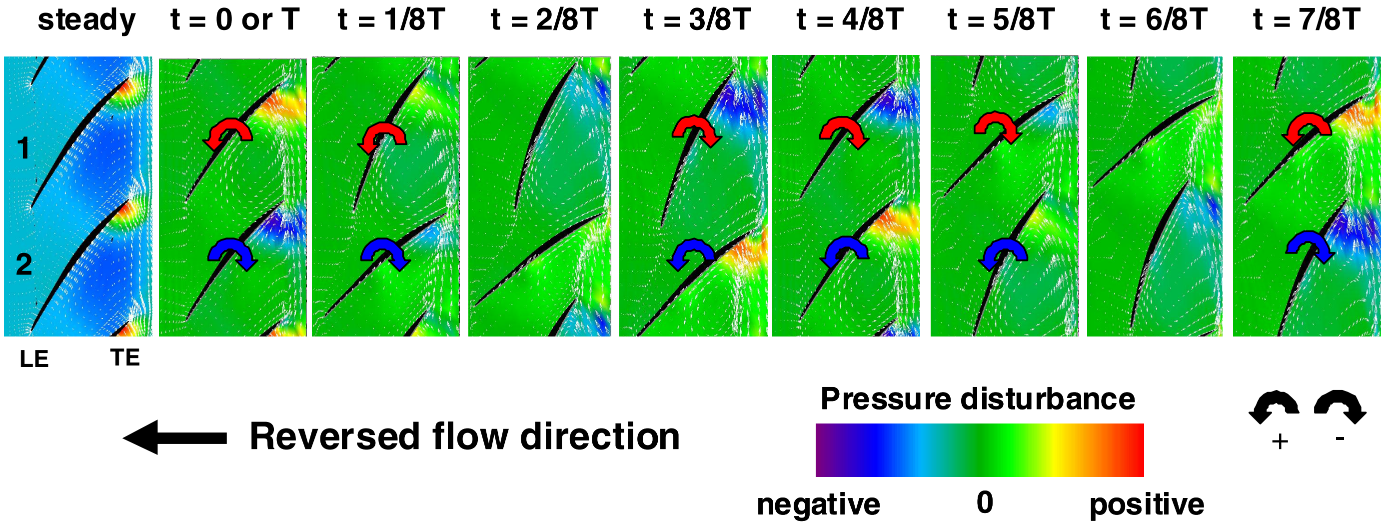

Figure 10: Pressure disturbance and flow vectors at p0 during backflow

At t=3/8T, a low pressure region is formed at the trailing edge of blade 1, exactly in-phase with the movement of blade 1 starting to go in negative direction, sucking the blade in this direction. At t=5/8T when the trailing edge of blade 2 reaches its uppermost position, a jet of fluid, starting at the trailing edge, goes into the direction of the pressure side of blade 1 and reaches this side at t=7/8T and t=T, creating a high pressure region at the trailing edge of blade 1, pushing it in positive direction. This is in phase with the movement of blade 1. Then, again the low pressure region at the trailing edge of blade 1 starts to occur at t=2/8T, starting a new vibration cycle.

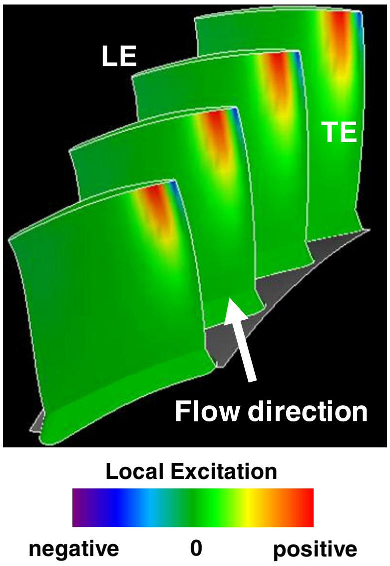

Figure 11: Local excitation during backflow conditions at p0 of the rotor

Thus, over a whole vibration period, work is done by the fluid onto the blade for this inter-blade phase angle, as is also shown in Figure 11. Here, the local excitation on the blade surface is shown, which corresponds to a negative aerodynamic damping. Red color indicates excitation (negative damping), while blue corresponds to positive damping. High negative damping can be observed in the tip region at about 10% chord length from the trailing edge, while the region with positive damping closer to the trailing edge is very small. The location of maximum negative damping coincides with the position of the steep pressure gradient in Figure 8.

Overall, the blade extracts work out of the flow at the reverse flow condition and is thus aerodynamically unstable for this inter-blade phase angle. This analysis shows that during reversed flow conditions compressor blades may be excited by flutter.

6 COMPARISON WITH MEASUREMENTS

During rig testing, blade vibrations were monitored with the tip-timing equipment, which was developed at MTU by Zielinski and Ziller [16], [17].

In Figure 12 a typical plot of the rotor blade tip deflections is shown. The green curve shows the original measured normalized deflections of the blade tip. The blue curve corresponds to averaged values and the red curve represents the deflections in the second vibration mode (1T). The time is referenced to the vibration period of the first torsion mode. In this plot, similar to that in Figure 1, a first excitation of the blade due to the pressure shock can be seen, starting at a relative time of 50 (which is not the topic of this paper). After this first blade loading, at a relative time of 110 the blade becomes aerodynamically unstable and the deflections start to grow with time. This period of time corresponds to operation of the rotor under reversed flow conditions as shown in Figure 3.

According to theory, an exponential growth rate is to be expected in case of blade flutter. Therefore, deflection data derived from the tip timing probes have been inspected to derive the growth behavior. Test data, as shown in Figure 12, actually allowed to determine the exponential growth of vibration amplitudes, as shown by the approximating black line in this figure. From the data, a vibration growth rate, in terms of the logarithmic decrement, could be deduced by fitting an exponential curve to the vibration data:

$$A = A_0 \cdot e^{-\delta \cdot f \cdot t} \tag{1}$$

From the measurements, a logarithmic decrement of the increasing vibration amplitude of about δ/δref = - 2.6 was obtained, using a curve fit according to eqn. (1).

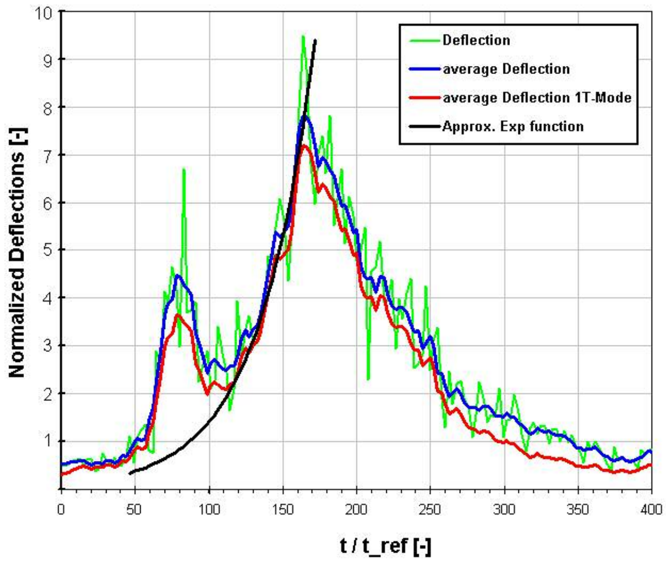

Figure 12: Measured rotor tip deflections during a surge cycle and fitted growth rate

In Figure 13, the calculated aerodynamic damping of the rotor blade is shown versus the dimensionless mass flow. Always the minimum damping from the damping curve as shown in Figure 14 is taken. All damping values are normalized with a reference damping due to proprietary reasons. Of course, this reference damping is the same for analytically and experimentally determined values. The change in damping is partly due to the different pressure level and partly due to changed flow conditions.

From rig testing, the mass flow during the surge blow-down phase could not be obtained, but a 1-D-analysis with an appropriate code [2] showed that this mass flow is expected to be in the range of -11% to -17% of the mass flow prior to surge. In the expected backflow regime the rotor is predicted to be unstable with a normalized logarithmic decrement somewhere between -2.3 and -3.0. The material damping is almost negligible. This fits very well with the experimentally observed behavior of this rotor blade.

Moreover, in the test it was observed that other rotor stages were unstable and some rotor stages stable. This behavior was predicted correctly by the analytical analysis.

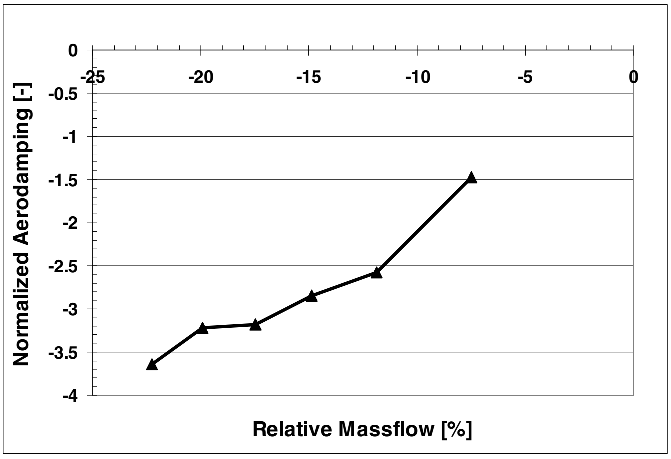

Figure 13: Normalized aerodynamic damping vs. relative mass flow rate for the rotor

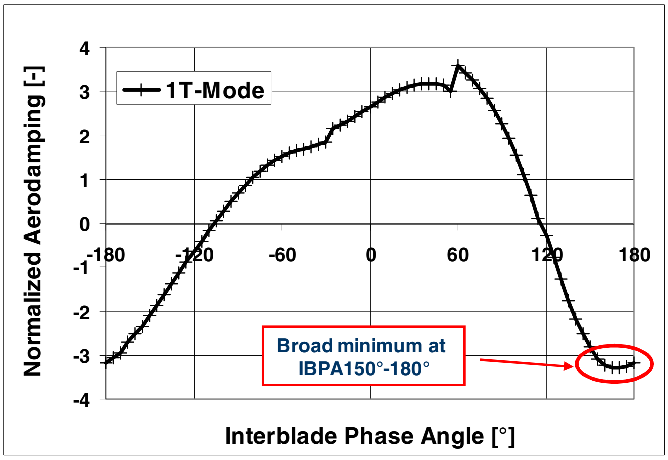

Figure 14: Calculated normalized aerodynamic damping vs. IBPA for the rotor

In Figure 14, the normalized aerodynamic damping of the first torsional mode of the rotor is plotted versus the interblade phase angle for performance point p0. It can be seen that the minimum damping does not occur at exactly 180°, but has a broader minimum at inter-blade phase angles of about 150°-180.

Figure 15 presents the corresponding results from the tip-timing measurements during the surge event. From the measured data, the excited IBPA of the rotor blades can be extracted. In this diagram of the vibration frequency f/f_{ref} (with $f_{ref}=f_{1T\text{-}Mode}$) versus time t/t_{ref} (with $t_{ref} = T_{1T\text{-}Mode}$) the color represents the level of vibration amplitude for all blades. The red and dark blue regions indicate the high vibrations during the surge event. It can be seen that at nodal diameters corresponding to an IBPA of 130°-170° the highest amplitudes occur, close to the region predicted by the numerical analysis.

The Figure shows an all-blade spectrum from the tip-timing analysis. The frequency on the y-axis is not the vibration frequency of the blade, but a frequency connected to the nodal diameter and speed. All vibration amplitudes are due to the first torsional mode.

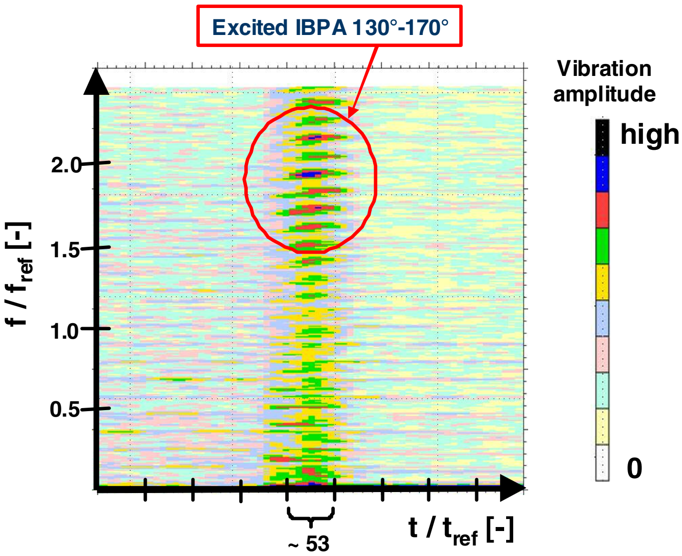

Figure 15: Tip-timing measurement results for the rotor

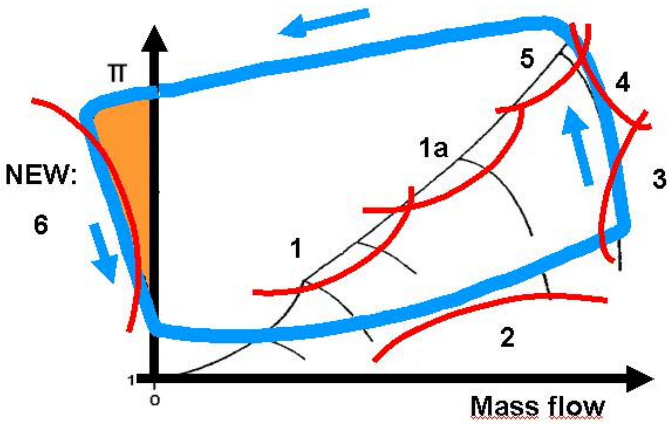

Figure 16: Compressor map with flutter regions

It should be noted that the complete surge cycle is a highly unsteady event and the performed investigations are based on quasi steady-state flow conditions. But for a typical vibration frequency of the first torsion mode of about 2 kHz and a backflow time of 50ms the blade may accumulate as much as 100 vibration periods, which may justify the quasi-steady assumption. Then, in eq. (1), assuming a log dec of -3% leads to a factor of e^3~20. If the initial stress after the hammershock is large enough, HCF failures may occur. Thus, even if in the first part of the paper it was shown that the calculation of unsteady pressure distributions at reversed flow conditions with the presented procedure gives reasonable results compared to the experiments, it is expected that the application to compressor surge has still some uncertainty and needs to be validated further.

However, the goal of this investigation was not to produce highly accurate numbers but to explain the fundamental physical phenomenon for the high blade vibrations in a qualitative way. The good agreement with the tip-timing measurements gives a high confidence that this goal was achieved with the presented work.

7 SUMMARY AND CONCLUSIONS

The work is summarized below and appropriate conclusions are drawn from the investigations:

- The quasi-steady state flow fields during the surge blow-down phase at several back pressures was computed with a 3D RANS code.
- Based on this complex flow field, aeroelastic flutter calculations with a linearized Euler code were performed.
- This aeroelastic analysis can explain blade failures during surge and its physical reason.
- The obtained numerical results compare well with measured observations during rig testing.
- Blade loads during a surge cycle may consist of two physically different phenomena in certain cases:

  1) The pressure wave which goes through the compressor when the flow breaks down. The excitation frequency is determined by the duration of the surge cycle and thus the volumes associated with the compressor.

  2) During the blow-down phase flow conditions can exist which are aerodynamically unstable and thus lead to flutter for some rotor stages. The duration of this condition is determined by the surge volume.

- A new flutter region in the compressor map was detected experimentally and analytically. In addition to the regions 1-5 as described by Sisto [18] and shown in Figure 16, a new flutter region 6 at reversed flow conditions was found, which may occur at certain circumstances:

1	Subsonic/transonic stall flutter
1a	System mode instability
2	Choke flutter
3	Low incidence supersonic flutter
4	High incidence supersonic flutter
5	Supersonic bending stall flutter
6	Reversed flow flutter

ACKNOWLEDGMENTS

The work published in this paper was partly funded by the German government (Lufo 4). This is gratefully appreciated.

REFERENCES

[1] Mazzawy, R. S., 1979, "Surge-Induced Structural Loads in Gas Turbines", ASME-paper 79-GT-91

[2] Schoenenborn, H.; Breuer, T.: „Aerodynamic and Mechanical Vibration Analysis of a Compressor Blisk at Surge", GT2004-53579, Proceedings of ASME Turbo Expo, June 2004, Vienna, Austria

[3] Simmons, H. R.; Brun, K.; Sastry, C.: "Aerodynamic Instability Effects on Compressor Blade Failure: A Root Cause Failure Analysis", GT2006-91353, Proceedings of ASME Turbo Expo, May 2006, Barcelona, Spain

[4] Vahdati, M.; Simpson, G.; Imregun, M.: „Unsteady Flow and Aeroelasticity Behaviour of Aero-Engine Core Compressors During Rotating Stall and Surge", GT2006-90308, Proceedings of ASME Turbo Expo, May 2006, Barcelona, Spain

[5] Mailach, R.; Vogeler, K.: "Unsteady Aerodynamic Blade Excitation at the Stability Limit and During Rotating Stall in an Axial Compressor", GT2006-90214, Proceedings of ASME Turbo Expo, May 2006, Barcelona, Spain

[6] Longley, J.P.: "Calculating Stall and Surge Transients", GT2007-27378, Proceedings of ASME Turbo Expo, May 2007, Montreal, Canada

[7] Gamache, R. N.; Greitzer, E. M.: "Reverse Flow in Multistage Axial Compressors", AIAA-paper 86-1747, AIAA/ASME/SAE/ASEE 22nd Joint Propulsion Conference, June 16-18, 1986, Huntsville, Alabama

[8] Frodl, V.: "Schaufelbelastung durch Pumpen in Verdichtern", VDI Fortschrittsberichte Nr. 259, Reihe 7: Strömungstechnik, ISBN 3-18-325907-9, 1995

[9] di Mare, L.; Krishnababu, S. K.; Mueck, B.; Imregun, M.: "Aerodynamics and aeroelasticity of a HP compressor during surge and reversed flow", Proceedings of the 12th ISUAAAT, Sept. 1-4, 2009, London, UK

[10] Eulitz, F., Engel, K., Nuernberger, D., Schmitt, S., Yamamoto, K.: "On Recent Advances of a Parallel Time-Accurate Navier-Stokes Solver for Unsteady Turbomachinery Flow", Proceedings of the 4th ECCOMAS, Papailiou et al., eds., John Wiley &Sons, Vol. 1, pp. 252-258, 1998.

[11] Nuernberger, D., Eulitz, F., Schmitt, S., Zachcial, A.: "Recent Progress in the Numerical Simulation of Unsteady Viscous Multistage Turbomachinery Flow", ISABE-2001-1081, 2001.

[12] Engel, K.; Zscherp, C.; Wolfrum, N.; Nuernberger, D.; Kuegeler, E.: "CFD Simulations of the TP400 IPC in Off-Design Operating Conditions", ASME-paper GT2009-60324, Orlando, Fl, USA, 2009

[13] Kahl, G.: "Application of the time linearized euler method to flutter and forced response calculations", ASME-paper 95-GT-123, Houston, Texas, June 5-8, 1995

[14] Kahl, G.; Klose, A.: "Computation of time linearized transonic flow in oscillating cascades", ASME-paper 93-GT-269, Cincinnati, Ohio, May24-27, 1993

[15] Schoenenborn, H.; Chenaux, V.; Ott, P.: "Aeroelasticity at reversed flow conditions - Part 1: Numerical and experimental investigations of a compressor cascade with controlled vibration", ASME-paper GT2011-45034, paper submitted

[16] Zielinksi, M.; Ziller, G.: „Noncontact blade vibration measurement system for aero engine application", ISABE, 17th International Symposium on Air Breathing Engines, Munich, Germany, September 4-9, 2005, paper no. 1220

[17] Zielinksi, M.; Ziller, G.: „Noncontact crack detection on compressor rotor blades to prevent further damage after HCF-failure", NATO RTO-AVT-121 Symposium on the Evaluation, Control and Prevention of HCF in Gas Turbine Engines, Granada, Spain, October 3-6, 2009, paper no. 19

[18] Sisto, F.: "Introduction and Overview", AGARD-Manual on Aeroelasticity in Axial-Flow Turbomachines Volume 1, AGARD-AG-298, Vol. 1, 1987